Original Article

Therapeutic potential of adipose-derived mesenchymal stem cell exosomes in tissue-engineered bladders

Journal of Tissue Engineering
Volume 12: 1–14

DOI: 10.1177/20417314211001545
journals.sagepub.com/home/tej
SAGE

Tianli Yang*, Feng Zhao*, Liuhua Zhou*, Jingyu Liu, Luwei Xu, Quanliang Dou, Zheng Xu and Ruipeng Jia

Abstract

Mesenchymal stem cells (MSCs) are a therapeutic tool for tissue engineering. However, many studies have recently shown that the therapeutic effects of MSCs are mediated by paracrine signaling and their secretory factors rather than their multidirectional differentiation ability. Exosomes isolated from the conditioned medium of MSCs are considered the main intercellular communication medium between MSCs and their target cells. Exosomes have been utilized in a novel cell-free therapy strategy that has attracted much attention. In this study, we evaluated the effects of a new cell-free tissue-engineered bladder (bladder acellular matrix combined with adipose-derived mesenchymal stem cell exosomes (AMEs)) in vivo and in vitro to prove that AMEs promoted tissue regeneration and functional recovery in a rat bladder replacement model.

Keywords

Bladder replacement, tissue engineering, mesenchymal stem cells, exosomes, bladder acellular matrix, angiogenesis

Received: 14 February 2021; accepted: 17 February 2021

Introduction

Bladder contracture or defects caused by numerous diseases require augmentation or replacement of the original bladder, and thus far, the gold standard of treatment is enterocystoplasty.[1] Nevertheless, the main function of the bowel mucosa is reabsorption and not storage. The differences in the microstructures between the bowel and urothelium may cause many complications, such as metabolic imbalance, lithogenesis, ileus, infection, and even malignant transformation.[2] Fortunately, the advent of bladder tissue engineering strongly supports the theoretical restoration of bladder structure and function. Traditional tissue engineering causes isolated and expanded cells to stick to a temporary scaffold and then proliferate and secrete their own extracellular matrix (ECM) to replace the biodegrading scaffold.[3] Recently, mounting evidence has proven that the therapeutic effects of stem cells are mainly due to the release of paracrine factors that subsequently promote numerous restorative processes.[4]

Extracellular vesicles (EVs) including apoptotic bodies, microvesicles, and exosomes, which are isolated with different methods, have been considered an important tool for intercellular communication.[5,6] Among them, exosomes are a subset of extracellular nanosized membrane vesicles with diameters ranging from 30 nm to 150 nm.[7] Their biogenesis occurs through the fusion of multivesicular bodies with the plasma membrane, releasing exosomes into the extracellular space.[8] Exosomes can carry molecules, such as DNA, RNA, proteins, and lipids, and directly reflect the metabolic state of the original cells.

To date, exosomes have been widely studied in the context of neoplasms. In fact, stem cell-derived extracellular vesicles have positive effects on tissue repair in many ways and can even reduce apoptosis caused by ischemic injury.[9] In recent years, many studies have confirmed the regenerative and reparative effects of exosomes secreted

Department of Urology, Nanjing First Hospital, Nanjing Medical University, Nanjing, China

*These authors have contributed equally to this work.

Corresponding author:
Ruipeng Jia, Department of Urology, Nanjing First Hospital, Nanjing Medical University, 68 Changle Road, Nanjing 210006, China.
Email: ruipengj@163.com

by adipose-derived mesenchymal stem cells (Ad-MSCs) in bone, skin, the brain, and the urethral epithelium.[10–13] The effects of tissue-engineered grafts rely on angiogenesis which originates from the homing of host endothelial cells (ECs) to the defect site, emphasizing the importance of migration and vascularization in tissue engineering.[14,15] Along with the graft being supplied with enough blood, necrosis, and contracture can be avoided.[16] Anderson et al.[17] first characterized the functional protein contents of MSCs and their exosomes, illuminating their beneficial effects in the clinic, and demonstrated that the MSC angiogenesis interactome is enriched for nodes associated with platelet-derived growth factor receptor (PDGFR), epidermal growth factor receptor (EGFR), and nuclear factor kappa B (NFκB). In recent studies, a multikinase complex called the IκB kinase (IKK) complex was considered a key point in the NFκB signaling pathway.[18] The phosphorylation of the IKK complex and IκB activated the NFκB pathway, whereas ammonium pyrrolidine dithiocarbamate (PDTC) prevented the degradation of IκB via the ubiquitylation-proteasome proteolytic pathway to inhibit the NFκB pathway.[19]

Adipose-derived mesenchymal stem cells and their exosomes can be obtained in large quantities since the source of fat is extensive and sufficient. Therefore, we speculated that bladder acellular matrix (BAM) combined with AMEs can effectively enhance tissue-engineered bladder regeneration and functional recovery by promoting vascularization. In this study, we evaluated AMEs in a so-called cell-free therapy to determine whether they promote bladder tissue regeneration and functional recovery in a rat bladder replacement model and explored the effect of the NFκB pathway on angiogenesis.

Materials and methods

Preparation of the BAM

BAM was prepared as previously described by our team.[20] In short, we trimmed the bladder sample and removed the fat tissue and fascia from its lumen. Then, we filled the bladder lumen with 100 mL of 0.25% trypsin/0.038% ethylenediaminetetraacetic acid (EDTA, Gibco) for incubation for 2 h at room temperature (RT). The bladder was then transferred into an ice-cold hypotonic solution overnight after washing with ice-cold PBS three times. Thereafter, the bladder was put into hypertonic solution and incubated for 24 h at RT. Finally, the bladder was incubated in 10 mM Tris buffer (pH = 7.6) containing 50 U/mL DNase I (Sigma-Aldrich), 1 U/mL RNase I (Sigma-Aldrich), 2 mM $MgCl_2$, 2 mM $CaCl_2$, and 150 mM NaCl for 24 h on an orbital shaker (150 r/min, Gesellschaft Fur Labortechnik) to remove all cell debris. The final BAM scaffold was obtained after three thorough washes with sterile ice-cold PBS lyophilization with a FreeZone 4.5 Liter Freeze Dry System (Labconco). The decellularized tissues were sterilized by ethylene oxide and stored at −20°C.

Quantification of total genomic DNA and sulfated GAGs

The quantification of total genomic DNA and sulfated GAGs was measured as our previous study.[21] In brief, samples of freeze-dried native porcine bladders and BAM were weighed, cut with scissors and digested with 50 mg/mL proteinase K (Merck) and RNase at 56°C overnight. Total genomic DNA was extracted via a DNA isolation kit for cells and tissues (Roche). After removing the protein precipitate, the remaining genomic DNA was collected and quantified with the Quant-iT™ PicoGreen® dsDNA Reagent and Kit (Invitrogen) according to the protocol. For the measurements of sulfated GAGs, the test solution was subjected to dimethylmethylene blue (Sigma-Aldrich) binding assay with absorbances at 525 nm. The amounts of DNA and sulfated GAGs were expressed as μg/mg dry weight of the test samples.

Histological analysis

Freeze-dried BAM was embedded in optimal cutting temperature (OCT) cryo-compound and then sliced into 6 μm sections. The tissue sections were immunofluorescently stained with primary antibodies against collagen I (COI, Abcam), collagen III (COIII, Abcam), fibronectin (Fn, Abcam), and laminin (La, Abcam) to confirm ECM preservation in the BAM.

Animals

A total of 30 male Sprague-Dawley (SD) rats and 20 male nude mice were used in this study. All animals were housed in facilities with free access to food and water in a standard room with constant temperature and humidity on a 12 h light/dark cycle. The experimental protocols were approved by the Institutional Animal Ethics Committee of the Affiliated Nanjing First Hospital of Nanjing Medical University and performed in accordance with the recommendations of experimental animals. The SD rats were divided into four groups: the subcutaneous transplantation BAM model group ($n = 5$), the subcutaneous transplantation BAM combined with AMEs model group (AMEs-BAM group, $n = 5$), the bladder replacement BAM model group ($n = 10$), and the bladder replacement AMEs-BAM model group ($n = 10$). The BAM scaffolds from the subcutaneous transplantation model were all harvested at 2 weeks, and the bladders from the animals in the bladder replacement model were harvested postoperatively at 4 and 12 weeks. The nude mice were divided into four groups for the Matrigel plug angiogenesis assay.

Ad-MSC extraction, characterization, and culture

First, we isolated the stromal vascular fraction (SVF) from epididymal adipose tissue as previously described.[22] Briefly, all rats were anesthetized for extraction of their epididymal adipose tissue, which was transported to the laboratory in ice-cold PBS (Gibco) as soon as possible. Then, we cut the adipose tissue into small pieces and mixed the pieces with 0.075%–0.1% type I collagenase at 37°C on a shaking table for 30–45 min. Next, we filtered the digested tissue through 200 μm nylon mesh and collected the filtrate. The filtrate was centrifuged at 400 g for 5 min to obtain the cells, including the SVF and blood cells. To purify the SVF, we used red blood cell lysis buffer to resuspend the cells for 5 min followed by centrifugation at 400 g for 5 min. Finally, the deposited cells were resuspended in Dulbecco's modified Eagle's medium (DMEM, Gibco) containing 10% fetal bovine serum (FBS, Gibco) in cell culture dishes, which were placed in a humidified incubator with 5% CO_2 and kept at 37°C. The DMEM was changed every other day, and then the third generation Ad-MSCs were transferred into mesenchymal stem cell medium (MSCM, ScienCell). Fourth-generation Ad-MSCs were used for subsequent experiments.

The fourth generation cells at 80–90% confluence were digested with 0.25% trypsin without EDTA (Invitrogen) and washed with PBS. The cell suspension (2×10^6 cells/mL) was prepared and dispensed into 10 1.5 mL Eppendorf tubes, and the following fluorescently labeled mouse anti-rat monoclonal antibodies were added: CD34-FITC (Bioss), CD45-PE (BioLegend), CD90-APC (BioLegend), CD106-PE (Bioss), and CD133-PE (Novus Biologicals).[23,24] The labeled Ad-MSCs were incubated for 30 min in the dark and then analyzed with a FACSCalibur instrument (BD Biosciences).

Osteoblast and adipocyte differentiation of Ad-MSCs

To test the multipotential properties of Ad-MSCs, we cultured them in different conditioned media.[24] In brief, fourth generation Ad-MSCs were cultured in two six-well plates with MSCM (ScienCell). The medium was changed to mesenchymal stem cell adipogenic differentiation medium (MADM, ScienCell) and mesenchymal stem cell osteogenic differentiation medium (MODM, ScienCell) when the cells reached 70–80% confluency. During the 3 weeks of culture, MADM and the MODM were exchanged every 3 days. Finally, all cells were fixed with methanol (−20°C, 2 min) and stained with Oil Red O and Von Kossa in accordance with the manufacturer's protocols (Abcam).[25] Stained cells were observed by inverted microscopy (Olympus).

Ad-MSC exosome extraction

Exosome-depleted FBS (System Bioscience) MSCM (10%) was used to culture fourth generation Ad-MSCs for 3 days, and then the supernatants were collected to extract the exosomes through ultracentrifugation (UC), which is considered the gold standard for extraction.[9] Briefly, the supernatants were centrifuged separately at 20,000 g for 30 min to remove debris and 110,000 g (4°C) for 70 min using a Ti90 rotor (Beckman Coulter) to collect the pellets.[26] All pellets were washed with 1× PBS and centrifuged at 110,000 g (4°C) for 70 min again to remove any contaminating proteins, and the remaining pellets, which were equal to the exosomes, were resuspended in 200 μL of PBS. The protein concentration of the exosomes was measured with a bicinchoninic acid (BCA) protein assay kit (Sigma-Aldrich).

Characterization of AMEs

For Western blot analysis (WB), MSC proteins and exosomes were added to 12% SDS-PAGE gels and transferred onto polyvinylidene fluoride membranes (PVDF membranes, Millipore), followed by blocking in 5% skim milk for 2 h at RT. Next, the membrane was incubated with diluted primary antibodies (anti-CD9 (BD Biosciences), anti-CD63 (BD Biosciences), anti-TSG101 (BD Biosciences), and anti-calnexin (BD Biosciences)) at 4°C on a shaker overnight. After three washes with Tris-buffered saline/Tween (TBST), the membrane was incubated with horseradish peroxidase-conjugated secondary antibody (Proteintech) at RT on a shaker for 2 h. Finally, the membranes were analyzed via the ChemiDoc™ XRS system (Bio-Rad).[27]

Transmission electron microscopy (TEM, Hitachi, Japan) was used to observe the morphology of the exosomes and take images. Nanoparticle tracking analysis (NTA) was performed by electrophoresis and Brownian motion video analysis laser scattering microscopy (Particlemetrix) to analyze the particle size, concentration and distribution, and the results were analyzed with ZetaView (ZetaView 8.04.02 software).

AMEs staining

Some exosomes were stained with PKH-26 Red Fluorescent Cell Linker Kits (Sigma-Aldrich) for follow-up experiments. The procedure was as follows: PKH-26 dye was diluted in diluent C to 8 μM (dye solution).[28] A sample of exosomes was mixed with the same volume of the dye solution for 5 min, and the residual dye solution was bound with 10% FBS in DMEM (Gibco). Then, the exosomes were pelleted by ultracentrifugation at 100,000 g for 70 min at 4°C (Beckman Coulter). Finally, the exosomes were resuspended in 400 μL of PBS and placed onto a 20% to 60% discontinuous sucrose gradient. The gradient was

ultracentrifuged at 100,000 g for 18 h at 4°C (Beckman Coulter). Each fraction was combined and diluted to 30 mL with Dulbecco's phosphate-buffered saline (DPBS). The exosomes were pelleted by ultracentrifugation at 100,000 g for 70 min at 4°C (Beckman Coulter) and then resuspended in the appropriate volume of PBS for use.

Tube formation assay

Each well of a prechilled μ-Slide angiogenesis plate (Ibidi) was covered with 10 μL of Matrigel (BD Biosciences) and incubated at 37°C for 30 min to form a layer.[29] Human umbilical vein endothelial cells (HUVECs) were suspended in serum-free endothelial cell growth medium (Basel) and seeded onto the former matrix at a density of 10,000 cells/well. There was one control group and three experimental groups, as follows: 1 μg/mL, 10 μg/mL, and 100 μg/mL AMEs, which were added 100 μL of AMEs at different concentrations (1×10^{11} particles, 1×10^{12} particles, and 1×10^{13} particles, respectively) to stimulate tube formation.[17] All plates were incubated at 37°C for 6 h in a 5% CO_2 humidified atmosphere and then observed by phase-contrast microscopy. The results were analyzed by ImageJ software (National Institutes of Health, Bethesda, MD, USA).

Cell migration and wound healing assay

HUVECs were seeded into the upper chamber containing a polycarbonate filter with a pore size of 8.0 μm (Corning) at a density of 100,000 cells per chamber with or without 10 μL AMEs (10 μg/mL, 1×10^{11} particles in 10 μL) and allowed to migrate at 37°C for 48 h, while lower chamber contained complete medium. After 48 h, nonmigrating cells on the upper layer were removed by a cotton swab, while migrated cells on the lower layer were fixed in 4% paraformaldehyde, stained with 0.1% crystal violet and captured by a microscope.

For the wound healing assay, prior to AMEs stimulation, HUVEC monolayers were scratched by a pipette tip after cells reached a complete confluency in six-well plates, washed twice with PBS to remove cell debris, and then treated with serum-free DMEM containing 100 μL AMEs (10 μg/mL, 1×10^{12} particles in 100 μL) for the indicated times (0, 12, and 24 h). Images were captured by an optical microscope and analyzed by ImageJ software.

Subcutaneous transplantation

Ten male SD rats were randomly divided into two groups for subcutaneous transplantation of the following materials: ethylene oxide-sterilized BAMs cut into 1 cm × 1 cm squares infiltrated with 250 μL of PBS and AMEs dyed with PKH-26 (2.5×10^{12} particles/stent). After 14 days, the grafts were excised and imaged. Half were embedded in OCT, immunohistochemically stained with anti-CD31 (Abcam) and counterstained with 4′,6-diamidino-2-phenylindole (DAPI, Vector Laboratories) for nuclear staining. The remaining grafts were used for enzyme-linked immunosorbent assay (ELISA).

Bladder replacement

These procedures were performed as described before.[29] Briefly, after anesthesia, each rat's peritoneum was incised to find the bladder. Following careful separation, the bladder was nearly 50% circumferentially excised at the dome of the bladder, avoiding the ureters. The residual bladder was sutured via the interrupted suture technique with the BAM using absorbable 6-0 polyglycolic acid sutures (Figure 6(a)). Antibiotics were used for 3 days after surgery.

Urodynamic test

After anesthesia, one side of a PE-50 polyethylene catheter was inserted into the bladder dome of each rat, and the other side was connected to a pressure sensor and an infusion pump via a three-way cock valve. The intravesical pressure gradually increased with a preheated sterile saline perfusion of the bladder at a velocity of 200 μL/min, and urination occurred when the critical pressure point was reached. The urination cycles of each rat were recorded to evaluate bladder compliance (threshold micturition pressure (ΔP)/maximal bladder volume (ΔV); ΔV/ΔP).

Immunofluorescence analysis

All rats were sacrificed by CO_2 to harvest a full bladder after 4 weeks and 12 weeks of experimentation, and the graft was fixed in 4% paraformaldehyde. The fixed specimens were dehydrated and embedded in paraffin for Masson staining, and the levels of urothelial-related proteins AE1/AE3, the contraction of smooth muscle marker alpha-smooth muscle actin (α-SMA, Abcam), and the levels of endothelial marker CD31 and neuronal marker S-100 (both from Abcam) were detected. By randomly selecting 10 independent fields of vision, we used ImageJ software (National Institutes of Health) to analyze the protein expression and vascular density.

Matrigel plug angiogenesis assay

Precooled growth factor-reduced Matrigel was mixed with 1 μg/mL and 10 μg/mL AMEs and 1 μg/mL AMEs combined with 10 μM PDTC at a ratio of 1:1.[17,30] To generate Matrigel plugs, 300 μL of this mixture was injected subcutaneously into the dorsal region of nude mice. After 2 weeks, a Drabkin's reagent kit (Sigma-Aldrich) was used to evaluate the hemoglobin content. ELISA was used to analyze the

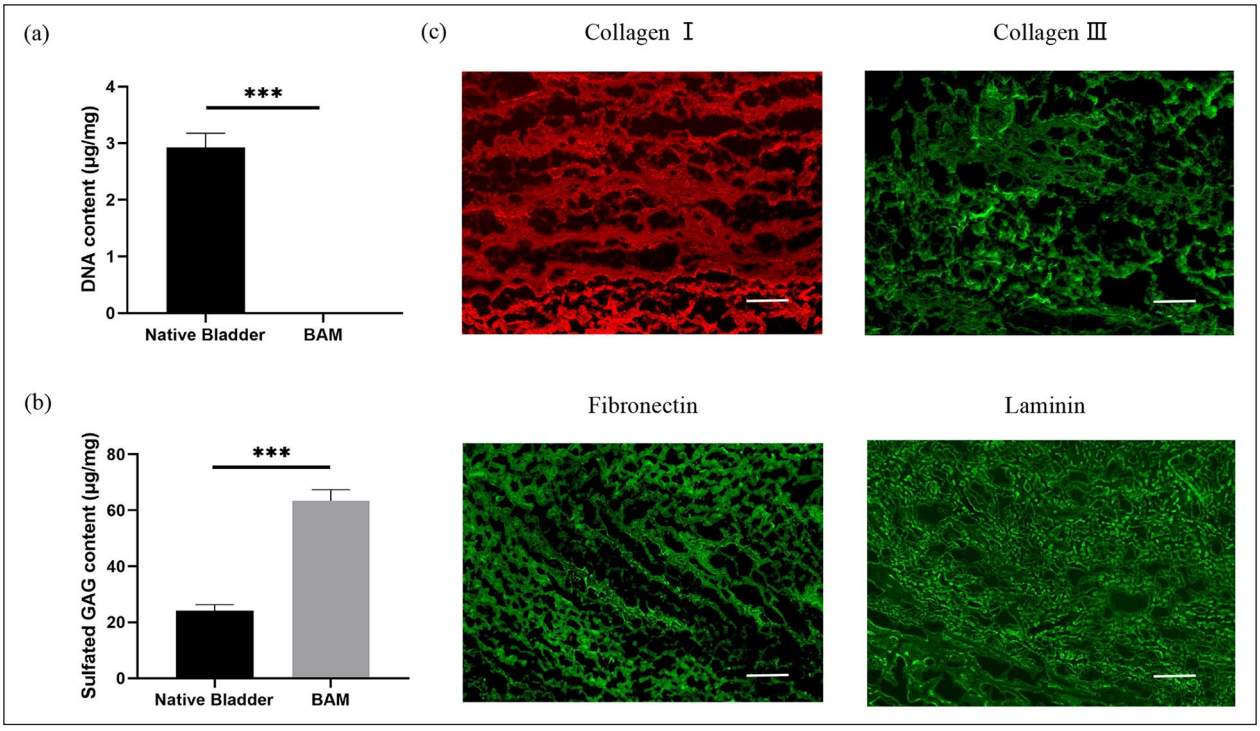

Figure 1. Characterization of BAM. (a) Quantification of DNA content in native porcine bladder and BAM. (b) Quantification of sulfated GAG content in native porcine bladder and BAM. (c) Immunofluorescence of BAM proteins (collagen I, collagen III, fibronectin, and laminin). Scale bar = 100 μm.
***$p < 0.001$.

expression of growth factors, and protocols described by the provider for PDGF-BB and VEGF (Cloud-Clone) were used for this assay. WB was performed as described previously to analyze the expression of NFκb-associative proteins, and the images were assessed via ImageJ software (National Institutes of Health).

Statistical analyses

Statistical analyses were performed with GraphPad Prism 8.0. All results are expressed as the mean ± standard deviation (standard deviation) and were analyzed by one-way ANOVA and independent Student's *t*-test. A value of $p < 0.05$ was considered statistically significant.

Results

Evaluation of BAM

There was no detectable DNA content in the BAM compared to the native porcine bladder and the content of sulfated GAG was significantly increased due to the loss of cellular materials after decellularization (Figure 1(a) and (b)). Immunofluorescent staining revealed that the components of the ECM, including collagen I, collagen III, fibronectin, and laminin, were well preserved in the BAM (Figure 1(c)).

Characterization of the Ad-MSCs

Flow cytometry analysis showed that the Ad-MSCs isolated from the Ad-SVFs expressed CD29, CD90, and CD106 but not CD34 and CD133 (Figure 2(a)). The expression of CD45 was positive upon isolation but lost in culture. Oil Red O staining showed that a large number of lipid droplets formed in the Ad-MSCs cultured in MADM for 21 days (Figure 2(b)), while Von Kossa staining revealed significant calcium salt deposition in the Ad-MSCs cultured in MODM for 21 days (Figure 2(c)), which proved the adipogenic and osteogenic differentiation abilities of Ad-MSCs.

Characterization of the AMEs

Ten microliters of AMEs was pipetted dropwise into the copper mesh for precipitation for 1 min, whereafter 10 μL of uranyl acetate was added to the copper net to settle for 1 min. After drying for a few minutes, the morphology of the AMEs was observed by TEM (Figure 2(d)), and the particle size distribution was analyzed by NTA (Figure 2(e)). As shown in the figure, most of the AMEs detected by NTA were in the range of 30–150 nm. Western blot analysis (Figure 2(f)) proved that the AMEs generally expressed CD9 (28 kDa, tetraspanins), CD63 (30 kDa, tetraspanins), and tumor susceptibility gene 101 (47 kDa,

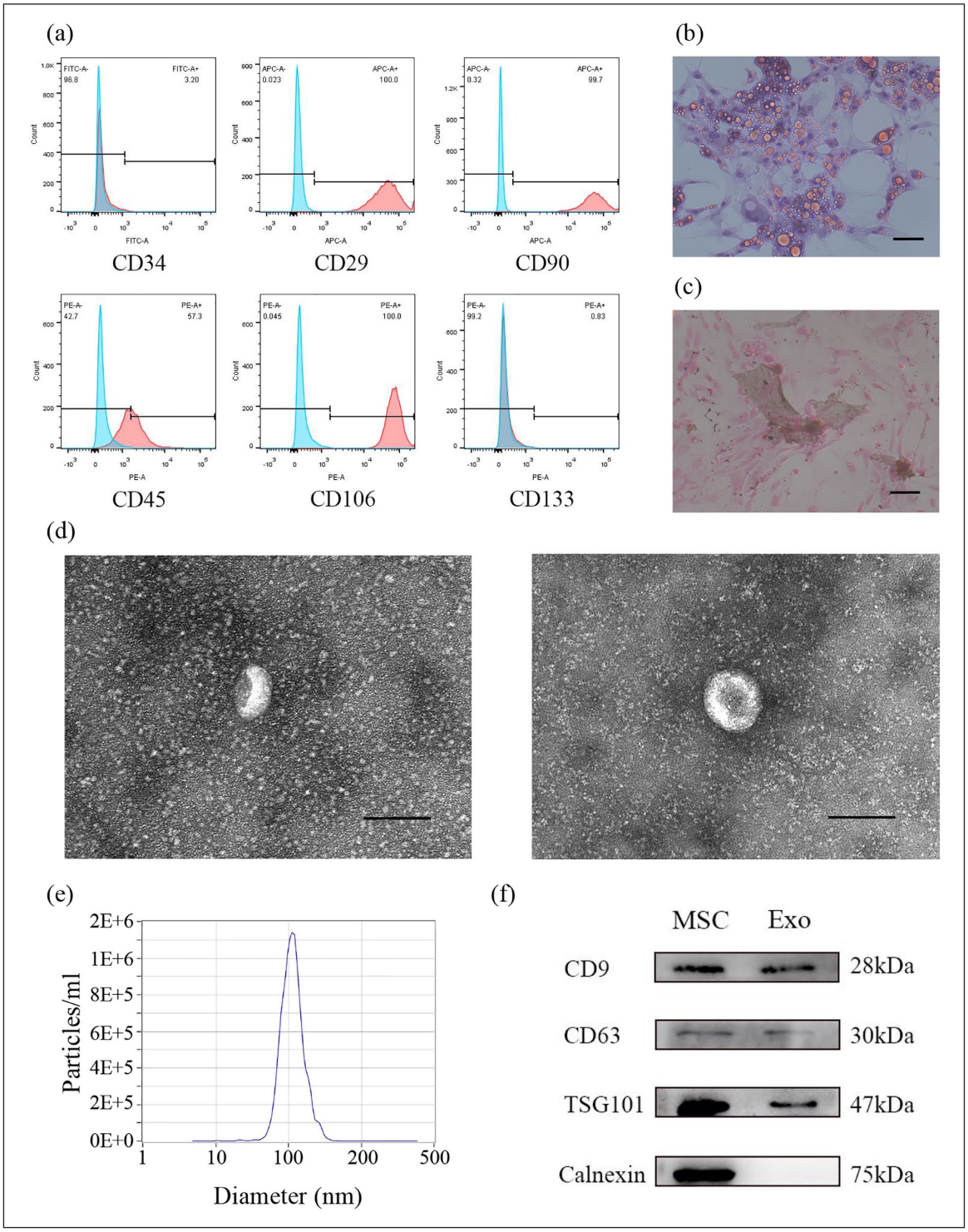

Figure 2. Identification of Ad-MSCs (a–c) and AMEs (d–f): (a) characterization of the fourth generation of Ad-MSCs was performed by flow cytometry, and the Ad-MSC histogram revealed that after purification, the cells mostly expressed mesenchymal cell markers. Differentiation assays showed that Ad-MSCs could differentiate into adipocytes (b) and osteocytes (c), which were stained with Oil Red O and Von Kossa, respectively. Scale bar = 100 μm. (d) TEM of exosomes isolated from MSCM-cultured Ad-MSCs for 3 days with 10% exosome-depleted FBS. Scale bars = 100 nm. (e) NTA found that most of these vesicles ranged in diameter from 30 to 150 nm. (f) Western blotting was performed with Ad-MSCs (MSCs) and AMEs (Exos). The expression of CD9, CD63, TSG101, and calnexin was detected.

Ad-MSCs: adipose-derived mesenchymal stem cells; AMEs: adipose-derived mesenchymal stem cell exosomes; NTA: nanoparticle tracking analysis; TEM: transmission electron microscopy.

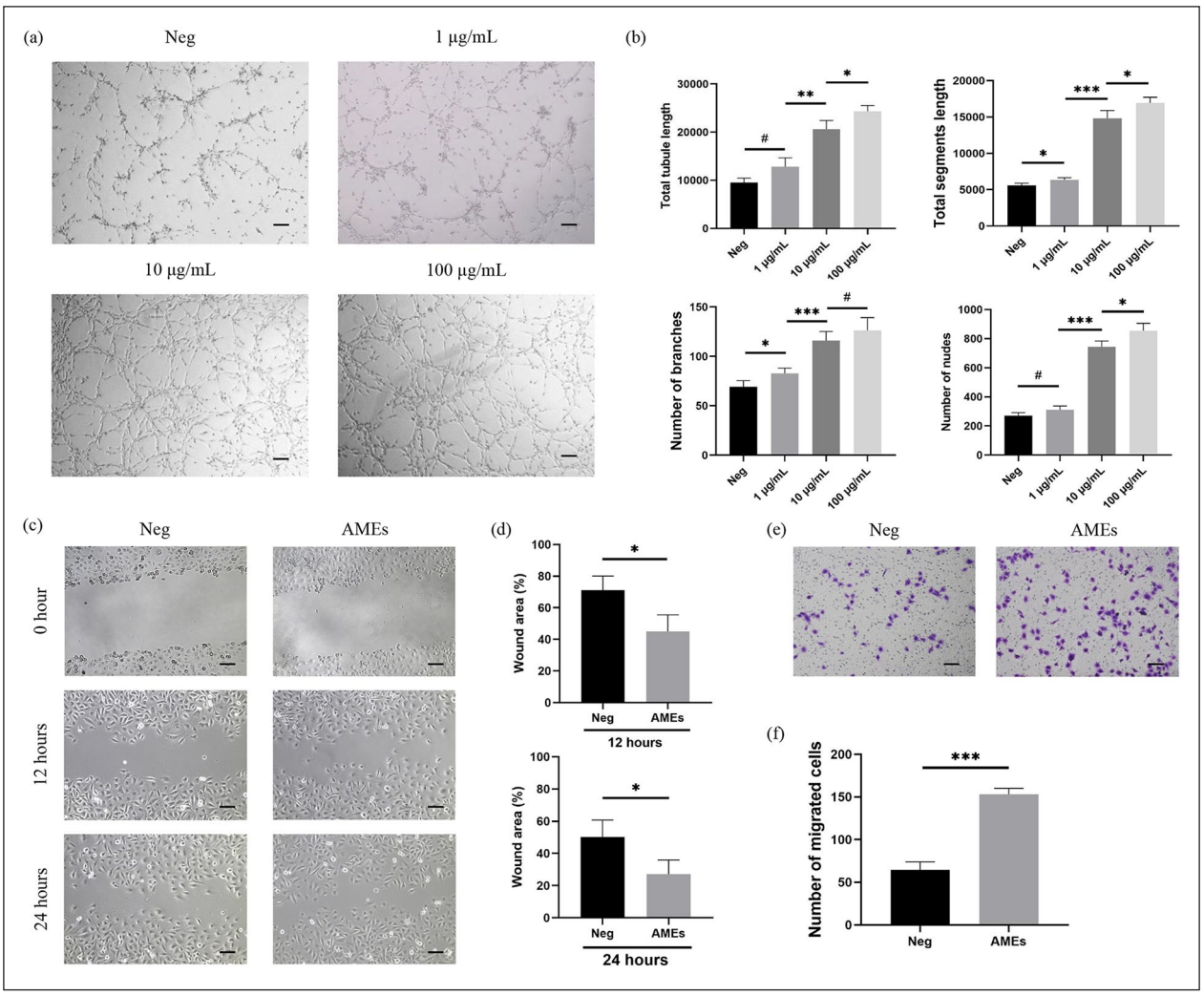

Figure 3. AMEs induced tubule formation (a–b) and migration (c–f) of HUVECs in vitro: (a): HUVECs were treated with basal media (Neg), 1 μg/mL AMEs, 10 μg/mL AMEs, and 100 μg/mL AMEs. Scale bar = 100 μm. (b) Quantification of total tubule length, total segment length, branches, and nudes was analyzed by ImageJ's angiogenesis plugin. Basal media contained 2% FBS. (c) HUVECs were scratched by a pipette tip and then treated with serum-free DMEM with or without 100 μL AMEs both for indicated times (0, 12, and 24 h). Scale bar = 100 μm. (d) The areas of wound healing at 12 h and 24 h were analyzed by ImageJ. (e) HUVECs were seeded with or without 10 μL AMEs into upper chamber containing a polycarbonate filter to migrate for 48 h. Scale bar = 100 μm. (f) The numbers of migrated HUVECs were counted by ImageJ.

FBS: fetal bovine serum; HUVECs: human umbilical vein endothelial cells.

*$p < 0.05$. **$p < 0.01$. ***$p < 0.001$.

#No significant difference compared with the BAM group.

TSG101) rather than calnexin (75 kDa, an endoplasmic reticulum), which is highly expressed by cells.[31]

Efficiency of AMEs angiogenesis

To select the effective concentration of AMEs for follow-up experiments, four different concentration gradients were studied in the tube formation assay in vitro. The medium dose (10 μg/mL, 1×10^{12} particles in 100 μL) of AMEs induced significant tubule formation compared to the control group and the low dose (1 μg/mL, 1×10^{11} particles in 100 μL) group (Figure 3(a)), as measured by total tubule length, total segment length, number of branches, and nudes (Figure 3(b)). The medium dose group used one-tenth the concentration of the high dose group but still significantly induced vascularization. Unfortunately, the high-dose (100 μg/mL, 1×10^{13} particles in 100 μL) group was considered more wasteful and less efficient, and here, we chose the medium dose (10 μg/mL) for follow-up experiments.

Migration analysis

The capacity of HUVEC migration was evaluated by Transwell and wound healing assays. Transwell assays

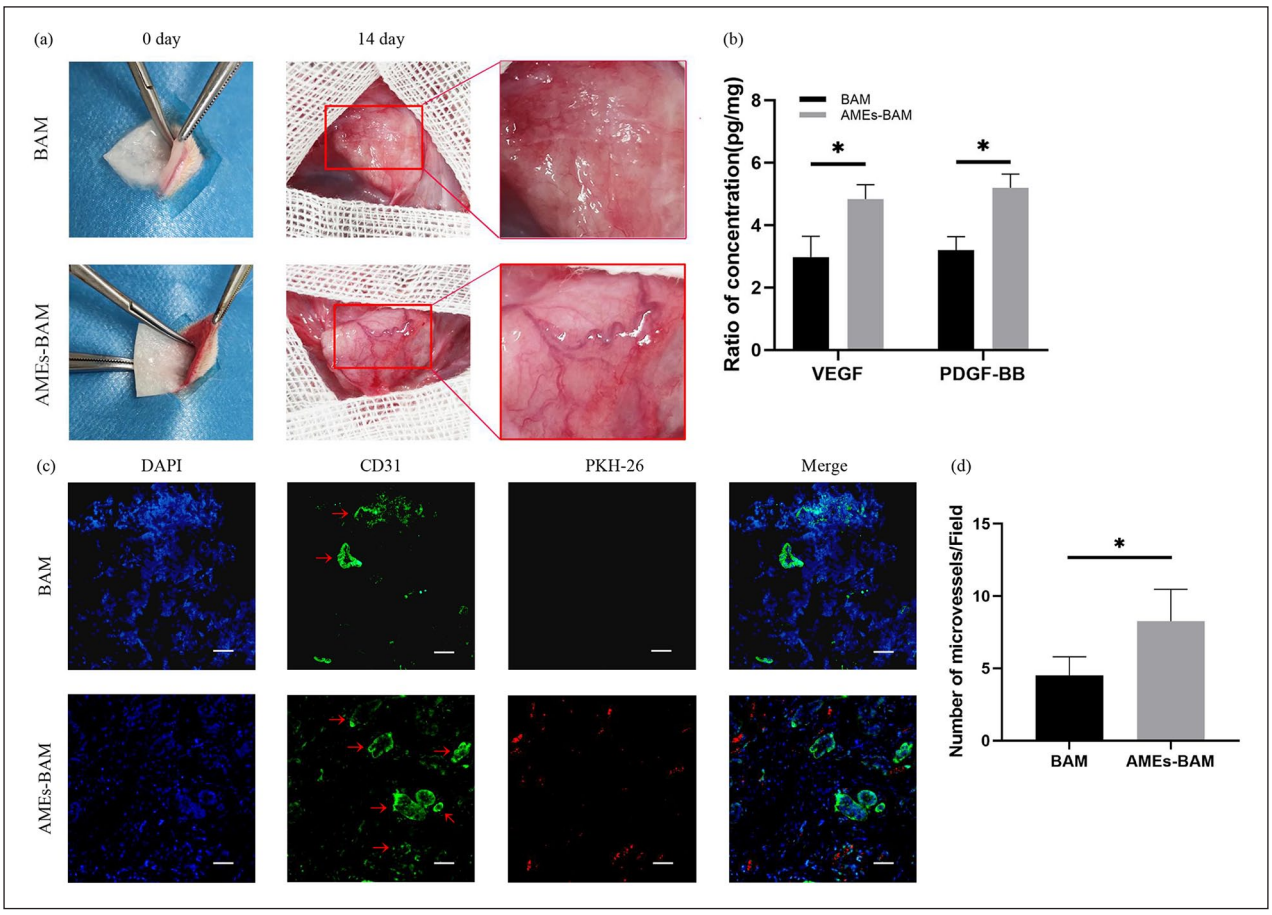

Figure 4. The subcutaneous transplantation model of AMEs-BAM: (a) BAM infiltrated with PBS or seeded with AMEs dyed by PKH-26 (250 μL/stent) was transplanted subcutaneously. (b) ELISA revealed that the expression of PDGF-BB and VEGF significantly increased in the AMEs-BAM group. (c) Immunohistochemical staining of transplanted BAM and AMEs-BAM. Nuclei were stained with DAPI (blue), microvessels were stained with CD31 (green) and AMEs were labeled with PKH-26 (red). All sections were observed by fluorescence microscopy. Representative microvessel structures are marked with arrows. Scale bar = 100 μm. (d) The number of microvessels per field was quantified.
ELISA: enzyme-linked immunosorbent assay.
*$p < 0.05$.

performed in the presence of 10 μg/mL AMEs presented a nearly twofold increase in the HUVEC migration ratio compared with negative group (Figure 3(e)). In addition, there was a significant difference between the 10 μg/mL AMEs-treated group and control group in the wound healing assay, suggesting that AMEs could promote HUVEC migration to induce the healing of wound area compared with the negative group (Figure 3(c)).

AMEs tracing

After 14 days, all materials were removed from the models of subcutaneous transplantation after anesthesia. Gross observations showed more obvious angiogenesis in the BAM stimulated by AMEs compared to simple BAM transplantation (Figure 4(a)). ELISA analysis of the remaining grafts showed that the levels of PDGF-BB and VEGF, which are considered classic growth factors of angiogenesis, were significantly increased in the AMEs-BAM group ($p < 0.05$ for both PDGF-BB and VEGF; Figure 4(b)). Immunofluorescence findings presented different degrees of cell proliferation, and the AMEs-BAM group showed a higher microvessel density per field than the BAM group (Figure 4(c)). AMEs were stained with PKH-26 before the establishment of the subcutaneous transplantation models, and the red labeling from PKH-26 was mostly located in the vascular region.

Gross analysis

Generally, rats with AMEs-loaded BAM presented better tolerance. Among all rats, only one rat in the sham group died because of urinary leakage before the end of the experiment. The gross appearances were not significantly different between the BAM group and the AMEs-BAM group at 4 weeks, whereas the AMEs-BAM group showed

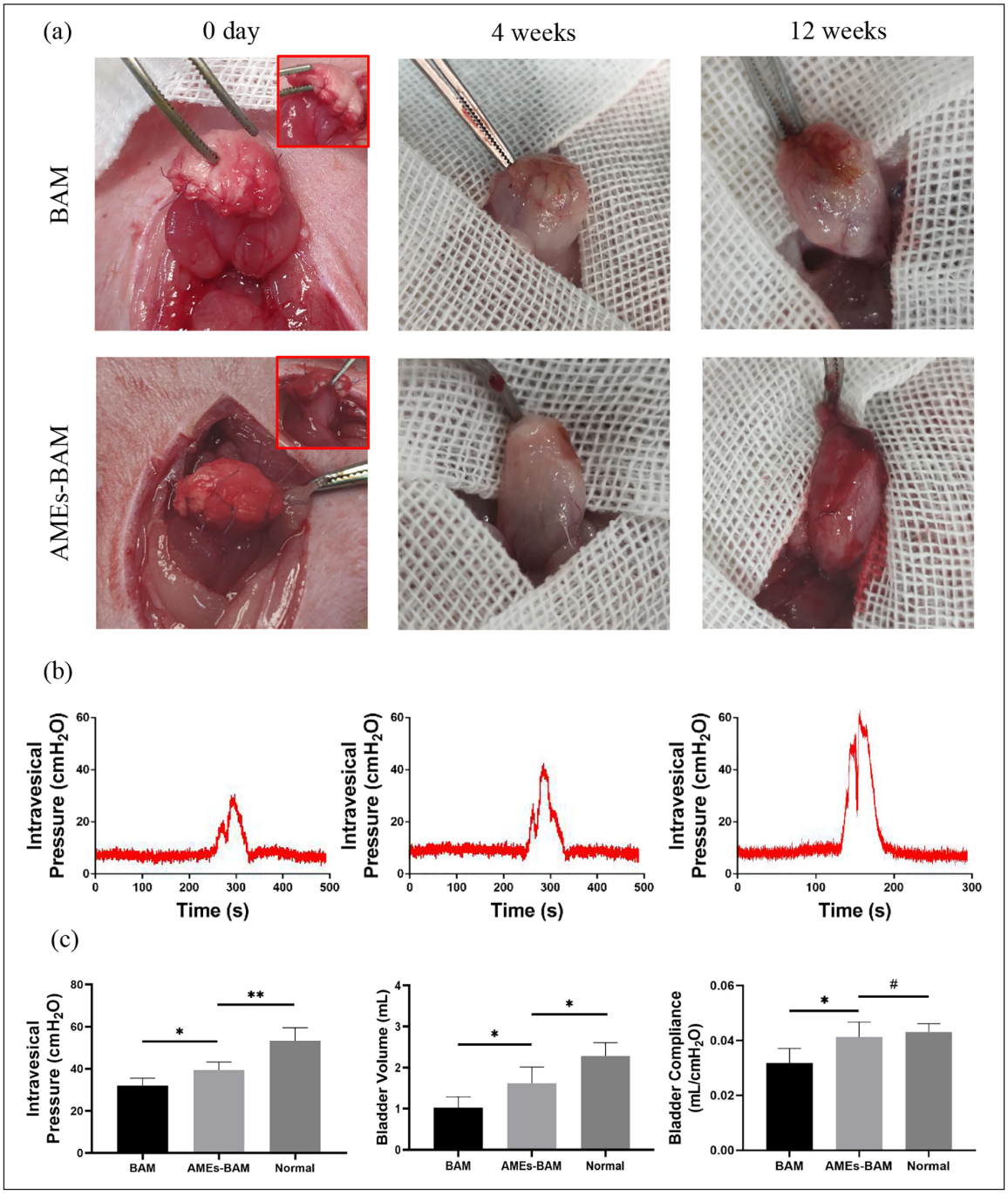

Figure 5. Establishment of bladder replacement model (a) and urodynamic parameters at 12 weeks after bladder replacement (b–c): (a) Gross observation of three phases of bladder replacement. (b) Representative intravesical pressure curves in the BAM, AMEs-BAM, and normal groups. (c) The intravesical pressure, bladder volume and bladder compliance of the BAM group were lower than those of the AMEs-BAM group.
*$p < 0.05$. **$p < 0.01$.
#No significant difference compared with the normal group.

greater morphology than the BAM group, which had an obvious graft contracture after 12 weeks (Figure 5(a)). Stone formation could barely be seen in both groups at 4 weeks; however, it could be observed to various degrees after 12 weeks. Vascularization of the AMEs-stimulated BAM was more obvious than that of the BAM alone.

Bladder compliance

Urodynamic tests were used to assess the function of the bladder replacement model (Figure 5(b)). Twelve weeks after the operation, the mean intravesical bladder pressure and mean bladder capacity (MBC) in the AMEs-BAM

group were significantly higher than those in the BAM group (Figure 5(c)). Moreover, the bladders of the rats in the AMEs-BAM group presented better compliance, showing no difference from the normal group.

Immunofluorescence analysis

Immunofluorescence was performed on all grafts to evaluate the expression levels of the urothelium marker AE1/AE3, the vascular-specific marker CD31, the smooth muscle marker α-SMA and the nerve marker S-100 at 4 weeks (Figure 6(a)) and 12 weeks (Figure 6(b)). The number and diameter of microvessels and the percentage of α-SMA-positive cells in the AMEs-BAM groups were significantly higher than those in the BAM groups (Figure 6(d)–(f)); however, the expression of AE1/AE3-positive cells and the number of nerves were not significantly different (Figure 6(c) and (g)). After 4 weeks, regeneration of the urothelium was almost complete. Notably, Masson staining showed significant differences between the samples at 12 weeks, and the degree of fibrosis was significantly decreased in the AMEs-BAM group (Figure 6(h)). After 12 weeks, the BAM combined with AMEs presented a higher density of CD31- and α-SMA-positive cells and a lower density of collagen fibers than BAM treatment alone.

Inhibitor of NFκB abrogates the angiogenic effects of AMEs

The NFκB pathway has been considered a potential effector role in angiogenesis.[32] To verify whether the presence of NFκB-associated proteins, such as IKK-α, IKK-β, and NFκB p65, promoted angiogenesis, AMEs were added to Matrigel with or without PDTC for the Matrigel plug assay (Figure 7(a)).[18] After 14 days, ELISA showed that the expression of PDGF-BB and VEGF was detectable in both the AMEs groups (1 μg/mL, 10 μg/mL) and the AMEs + PDTC groups. However, the levels of PDGF-BB and VEGF significantly decreased in the AMEs + PDTC groups ($p < 0.05$ for PDGF-BB and VEGF; Figure 7(b)). Quantification of angiogenesis within the Matrigel plugs showed that PDTC significantly suppressed the angiogenic effects of AMEs via blockade of the NFκB pathway ($p < 0.001$; Figure 7(c)). Compared to the Matrigel plugs without PDTC, the relative content of hemoglobin of those with PDTC was decreased by nearly 45%. The expression of IKK-α/β increased when the NFκB pathway was inhibited, whereas the expression of NFκB p65 increased when the pathway was activated (Figure 7(d)). The administration of PDTC significantly suppressed the activation of the IKK-α/β complex; thus, the IKK-α/β/NFκB pathway was inhibited.

Discussion

Extracellular vesicles (EVs), with diverse and nanoscale membranes, are actively released by cells.[33] Based on their size, biogenesis, and biophysical properties, they can be further classified as exosomes, microvesicles, or apoptotic bodies. Currently, EVs are known by scholars to come from cellular debris and thus were once underestimated to be important vehicles of intercellular communication.[34] Among these vesicles, MSC-derived exosomes, containing cytokines, growth factors, and regulatory miRNAs, have been studied due to their promising prospects in regenerative medicine.[35]

As the safety and efficacy of MSC-derived exosomes for angiogenesis of diseased organs, such as kidney, peripheral arterial, skin, and spinal cord, have been reported in recent studies, we hypothesized that exosomes extracted from Ad-MSCs that were abundant in fat tissue would be suitable for the construction of tissue-engineered bladders.[17,36–38] Our study first revealed the therapeutic potential of AMEs in tissue-engineered bladders. Compared to traditional stem cell transplantation, AMEs-seeded scaffolds represent a new cell-free therapy that can overcome certain drawbacks of stem cell therapy. Despite the complexity and high cost of exosome preparation, their advantages, such as controllability, safety, and high efficiency, make them valuable.

Ju et al.[39] supported that cardiac MSC-derived exosomes (C-MSC-Exos) had the potential to improve blood perfusion in the ischemic hindlimb region because of the high abundance of miR-7116-5p contained within C-MSC-Exos. Komaki et al.[40] showed the proangiogenic ability of human term placental tissue-derived MSC exosomes (PlaMSC-Exos) in a murine auricle ischemia model. Additionally, Harrell et al.[41] reported that MSC-derived EVs enriched with bioactive molecules suppressed the immune response and promoted regeneration efficiently by regulating the phenotype and function of immune cells. In our study, we started with cell cultures to establish a bladder replacement model that contained AMEs-loaded BAM. As shown in the results above, AMEs significantly improved the recovery of bladder function and morphology. Histologically, the advantages of AMEs have been their use in the regeneration of blood vessels and smooth muscles in tissue-engineered bladders, especially regarding angiogenesis.

To date, the tissue-engineered bladder research field has used different scaffolds or different cells combined with different scaffolds. Sharma et al.[42] MSCs transduced with green fluorescent protein (GFP) were seeded onto small intestinal submucosa (SIS) scaffolds to establish a bladder augmentation model. In our previous study, we successfully constructed a vascularized bladder with autologous adipose-derived stromal vascular fraction cells combined with BAM.[29] Undoubtably, these methods for tissue engineering have significant effects; however, the cells used require preservation of their viability and function from culture to storage and delivery. Hence, unlike cells, AMEs can be easily filtered and stored in a sterile manner, and their retention in the host tissue is quite short.

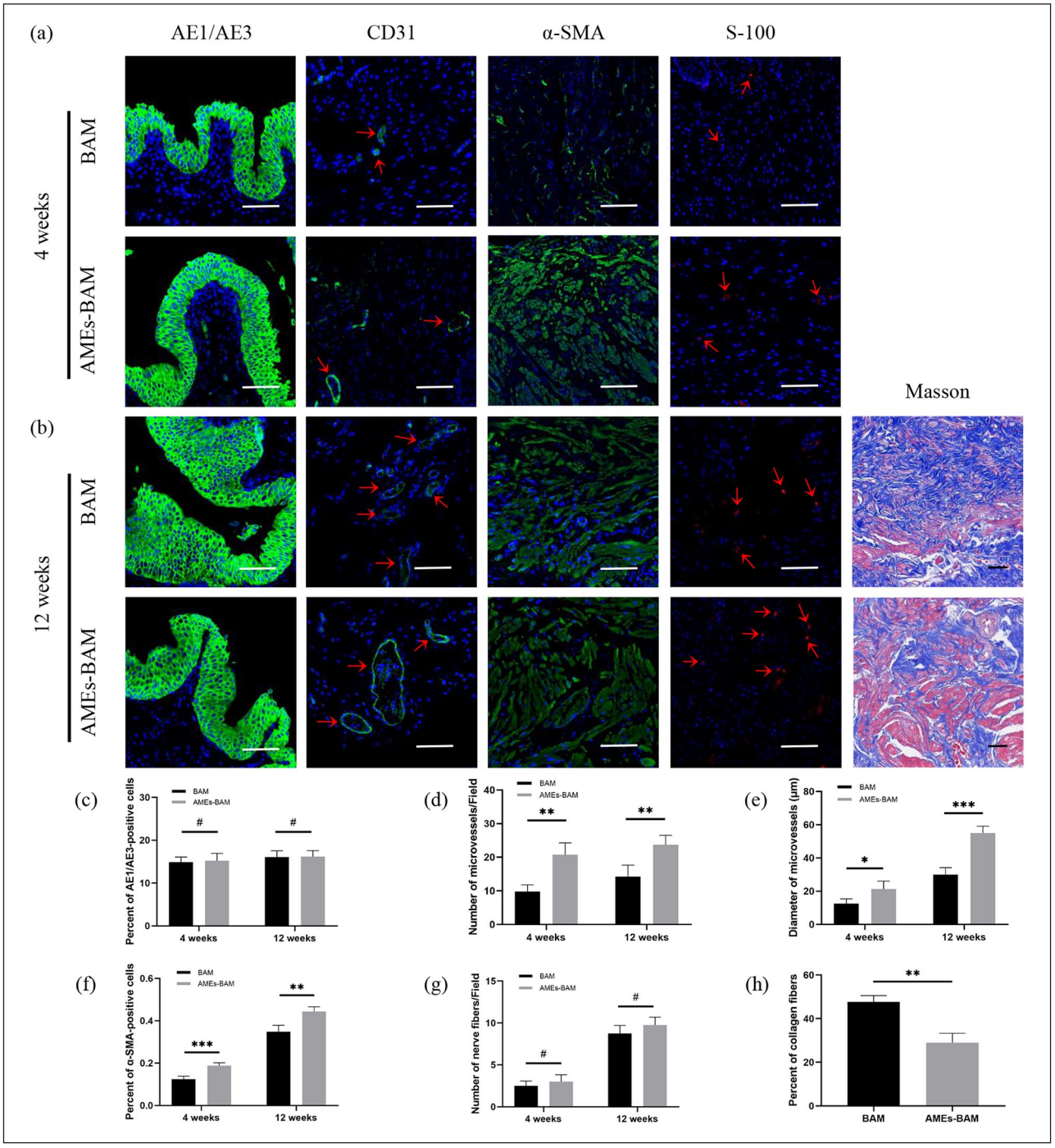

Figure 6. Immunofluorescence of all grafts: (a) Photomicrographs of urothelial markers and nuclei (AE1/AE3 + DAPI), blood vessel endothelial markers and nuclei (CD31 + DAPI), smooth contractile muscle markers and nuclei (α-SMA + DAPI) and neuronal markers and nuclei (S-100 + DAPI) in all groups at 4 weeks after replacement. Scale bar = 100 μm. (b) Photomicrographs of AE1/AE3 + DAPI, CD31 + DAPI, α-SMA + DAPI, S-100 + DAPI, and Masson staining in all groups at 12 weeks after replacement. Scale bar = 100 μm. (c–g) Quantification analysis showed that the regeneration of vessels and smooth muscles in the AMEs-BAM group was significantly better than that in the BAM group, whereas the urothelium and nerves were not significantly different. (h) Quantification analysis indicated that the fibrosis of the AMEs-BAM group at 12 weeks was obviously alleviated compared to that of the BAM group.

α-SMA: alpha-smooth muscle actin.

*$p < 0.05$. **$p < 0.01$. ***$p < 0.001$.

#No significant difference compared with the BAM group.

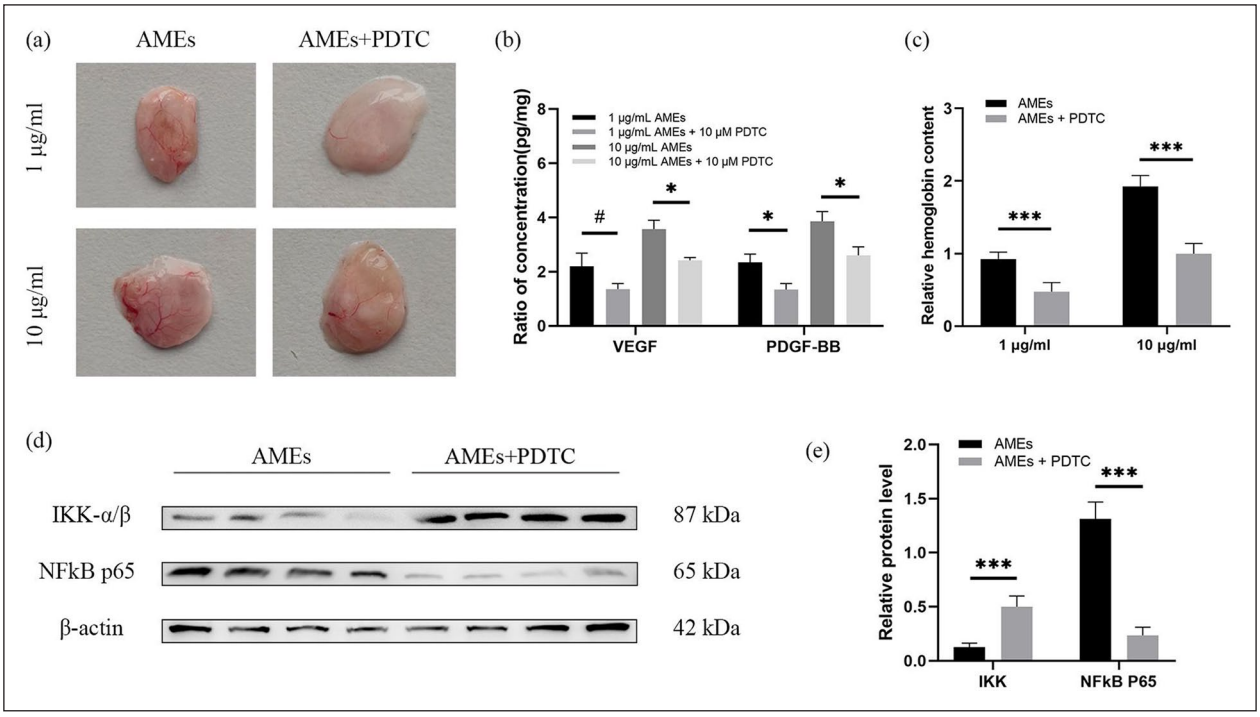

Figure 7. NFκB inhibition suppressed AMEs-mediated Matrigel plug angiogenesis in vivo: (a) Gross observation of Matrigel plugs, 50 μL AMEs (1 μg/mL and 10 μg/mL) mixed with 250 μL Matrigel, 50 μL AMEs (1 μg/mL and 10 μg/mL) mixed with 50 μL PDTC (10 μM) and 200 μL Matrigel. (b) ELISA revealed that the expression of PDGF-BB and VEGF significantly decreased after PDTC was added. (c) Quantification of the angiogenesis of the Matrigel plugs presented under all conditions. (d, e) The expression of IKK-α/β in the AMEs + PDTC group increased, while the expression of NFκB p65 decreased.
IKK: IκB kinase; NFκB: nuclear factor kappa B; PDTC: ammonium pyrrolidine dithiocarbamate.
*$p < 0.05$. ***$p < 0.001$.
#No significant difference compared to the 1 μg/mL AMEs group.

Moreover, the controllable concentration of AMEs in vitro indicates their safety and efficiency. According to our tube formation assay, we found that 10 μg/mL AMEs induced significantly greater tubule formation than 0 and 1 μg/mL AMEs, whereas 100 μg/mL AMEs were more wasteful and less efficient, considering the cost of AMEs extraction. Then we verified the effect of AMEs on EC migration, and as expected, AMEs significantly enhanced the migration ability of ECs which was vital to tissue repair and regeneration via Transwell and wound healing assays.

Based on the above research, we established subcutaneous transplantation models to track the retention of PKH-26-labeled AMEs. The labeled AMEs persisted after 2 weeks and participated in vascularization. Twelve weeks after replacement, the extent of regeneration of the blood vessels and smooth muscles in the AMEs-loaded BAMs was improved according to immunofluorescence analysis. By contrast, replacement with BAM alone was less than satisfactory. Although immunofluorescence assessment showed no significant difference between the regeneration of the urothelium and nerve fibers compared to the same period, there was some improvement after another half month. Notably, Masson staining revealed a great alleviation of fibrosis in the AMEs-BAM group at 12 weeks. Among urothelium, blood vessels, smooth muscles, and nerve fibers, the regeneration of the urothelium was the earliest and the easiest, while nerve fibers were opposite. Compared to the BAM group, the mean bladder capacity in the AMEs-BAM group increased by approximately 40%, whereas the capacity in both groups was still significantly smaller than that in the normal group. The urodynamic test showed that the mean intravesical pressure decreased to some degree. Compared to the BAM group, the mean bladder compliance in the AMEs-BAM group was close to that of the normal bladder. Above all, these results proved that using AMEs-loaded BAM to reconstruct bladder defects is a promising method for bladder engineering.

During regenerated bladder angiogenesis, some AMEs signaling pathway proteins are important mediators. Anderson et al.[17] first identified 1927 proteins in MSC-derived exosomes and filtered several paracrine effectors relevant to angiogenesis, such as EGF, PDGF, FGF, and NFκB, via multilayered analyses. The results of the tube formation assay indicated that an effective dosage range existed. Hou et al.[32] examined the functions of IKK-β in angiogenesis during mouse development. We investigated the effects of NFκB on AMEs angiogenesis since PDTC significantly decreased the hemoglobin content compared to

that in the AMEs groups. In addition, the expression levels of PDGF-BB, VEGF, and NFκB p65 significantly decreased when PDTC blocked the NFκB pathway, whereas the expression of IKK-α/β increased. These results indicate that NFκB signaling, which is a known classical proinflammatory pathway, plays an important role in vascularization.[43]

In the present study, we first introduced stem cell-derived exosomes for bladder tissue engineering and proved that the administration of AMEs could alleviate BAM fibrosis while it could also stimulate and induce BAM angiogenesis, which was of great benefit to the regeneration and construction of the bladder. In in vitro and in vivo experiments, we verified the appropriate concentration of AMEs and the highly relevant NFκB signaling profile. Twelve weeks after surgery, almost all animals survived, and the AMEs-BAM group presented a greater tolerance than the BAM group. Immunofluorescence assessment showed that the blood vessels and smooth muscles of the rats in the AMEs-BAM group regenerated better than those in the BAM group.

Conclusion

Herein, we introduced a novel cell-free therapy in place of previous traditional bladder engineering therapy. Using AMEs can avoid certain drawbacks of the use of cells directly. However, this cell-free therapy is faced with complexity and a high cost of preparation. To make this experiment receivable, we only utilized AMEs as a variable when there was a great variety of scaffolds with increased research. In our study, we proved that AMEs-loaded BAMs accelerated bladder regeneration through the promotion of vascularization through NFκB signaling. Overall, AMEs as the seeds of cell-free therapy have a promising future for tissue-engineered bladders.

Declaration of conflicting interests

The author(s) declared no potential conflicts of interest with respect to the research, authorship, and/or publication of this article.

Funding

The author(s) disclosed receipt of the following financial support for the research, authorship, and/or publication of this article: This work was supported by the National Natural Science Foundation of China (31500785, 81570613, 81902602, 92049111), Jiangsu Provincial Social Development Project (BE2017615), Jiangsu Provincial Medical Youth Talent (QNRC2016071), Nanjing Medical Science and Technology Development Project (JQX17007, ZDX16006), and Science and Technology Foundation from Nanjing Medical University (NMUB2018316).

ORCID iDs

Tianli Yang https://orcid.org/0000-0002-0314-8495
Feng Zhao https://orcid.org/0000-0001-7111-4812

References

1. Budzyn J, Trinh H, Raffee S, et al. Bladder augmentation (enterocystoplasty): the current state of a historic operation. *Curr Urol Rep* 2019; 20(9): 50.
2. Martini A, Villari D and Nicita G. Long-term complications arising from bowel interposition in the urinary tract. *Int J Surg* 2017; 44: 278–280.
3. Park KD, Kwon IK and Kim YH. Tissue engineering of urinary organs. *Yonsei Med J* 2000; 41(6): 780–788.
4. Mirotsou M, Jayawardena TM, Schmeckpeper J, et al. Paracrine mechanisms of stem cell reparative and regenerative actions in the heart. *J Mol Cell Cardiol* 2011; 50(2): 280–289.
5. Yáñez-Mó M, Siljander PR, Andreu Z, et al. Biological properties of extracellular vesicles and their physiological functions. *J Extracell Vesicles* 2015; 4: 27066.
6. Todorova D, Simoncini S, Lacroix R, et al. Extracellular vesicles in angiogenesis. *Circ Res* 2017; 120(10): 1658–1673.
7. Gurunathan S, Kang MH, Jeyaraj M, et al. Review of the isolation, characterization, biological function, and multifarious therapeutic approaches of exosomes. *Cells* 2019; 8(4): 307.
8. Harding C, Heuser J and Stahl P. Receptor-mediated endocytosis of transferrin and recycling of the transferrin receptor in rat reticulocytes. *J Cell Biol* 1983; 97(2): 329–339.
9. Bjørge IM, Kim SY, Mano JF, et al. Extracellular vesicles, exosomes and shedding vesicles in regenerative medicine - a new paradigm for tissue repair. *Biomater Sci* 2017; 6(1): 60–78.
10. Li W, Liu Y, Zhang P, et al. Tissue-engineered bone immobilized with human adipose stem cells-derived exosomes promotes bone regeneration. *ACS Appl Mater Interfaces* 2018; 10(6): 5240–5254.
11. Choi EW, Seo MK, Woo EY, et al. Exosomes from human adipose-derived stem cells promote proliferation and migration of skin fibroblasts. *Exp Dermatol* 2018; 27(10): 1170–1172.
12. Otero-Ortega L, Gómez de Frutos MC, Laso-García F, et al. Exosomes promote restoration after an experimental animal model of intracerebral hemorrhage. *J Cereb Blood Flow Metab* 2018; 38(5): 767–779.
13. Ni J, Li H, Zhou Y, et al. Therapeutic potential of human adipose-derived stem cell exosomes in stress urinary incontinence - an in vitro and in vivo study. *Cell Physiol Biochem* 2018; 48(4): 1710–1722.
14. Xing J, Jin H, Hou T, et al. Establishment of a bilateral femoral large segmental bone defect mouse model potentially applicable to basic research in bone tissue engineering. *J Surg Res* 2014; 192(2): 454–463.
15. Li Z, Yang A, Yin X, et al. Mesenchymal stem cells promote endothelial progenitor cell migration, vascularization, and bone repair in tissue-engineered constructs via activating CXCR2-Src-PKL/Vav2-Rac1. *FASEB J* 2018; 32(4): 2197–2211.
16. Nunes SS, Maijub JG, Krishnan L, et al. Generation of a functional liver tissue mimic using adipose stromal vascular fraction cell-derived vasculatures. *Sci Rep* 2013; 3: 2141.
17. Anderson JD, Johansson HJ, Graham CS, et al. Comprehensive proteomic analysis of mesenchymal stem cell exosomes reveals modulation of angiogenesis via nuclear factor-kappaB signaling. *Stem Cells* 2016; 34(3): 601–613.

18. Contreras-Nuñez E, Blancas-Flores G, Cruz M, et al. Participation of the IKK-α/β complex in the inhibition of the TNF-α/NF-κB pathway by glycine: possible involvement of a membrane receptor specific to adipocytes. *Biomed Pharmacother* 2018; 102: 120–131.
19. Li YQ, Zhang ZX, Xu YJ, et al. N-Acetyl-L-cysteine and pyrrolidine dithiocarbamate inhibited nuclear factor-kappaB activation in alveolar macrophages by different mechanisms. *Acta Pharmacol Sin* 2006; 27(3): 339–346.
20. Zhou L, Yang B, Sun C, et al. Coadministration of platelet-derived growth factor-BB and vascular endothelial growth factor with bladder acellular matrix enhances smooth muscle regeneration and vascularization for bladder augmentation in a rabbit model. *Tissue Eng Part A* 2013; 19(1–2): 264–276.
21. Yang B, Zhang Y, Zhou L, et al. Development of a porcine bladder acellular matrix with well-preserved extracellular bioactive factors for tissue engineering. *Tissue Eng Part C Methods* 2010; 16(5): 1201–1211.
22. Zhou L, Xu L, Shen J, et al. Preischemic administration of nonexpanded adipose stromal vascular fraction attenuates acute renal ischemia/reperfusion injury and fibrosis. *Stem Cells Transl Med* 2016; 5(9): 1277–1288.
23. Mushahary D, Spittler A, Kasper C, et al. Isolation, cultivation, and characterization of human mesenchymal stem cells. *Cytometry A* 2018; 93(1): 19–31.
24. Ciuffreda MC, Malpasso G, Musarò P, et al. Protocols for in vitro differentiation of human mesenchymal stem cells into osteogenic, chondrogenic and adipogenic lineages. *Methods Mol Biol* 2016; 1416: 149–158.
25. Ning J, Li C, Li H, et al. Bone marrow mesenchymal stem cells differentiate into urothelial cells and the implications for reconstructing urinary bladder mucosa. *Cytotechnology* 2011; 63(5): 531–539.
26. Helwa I, Cai J, Drewry MD, et al. A comparative study of serum exosome isolation using differential ultracentrifugation and three commercial reagents. *PLoS One* 2017; 12(1): e0170628.
27. Schneider CA, Rasband WS and Eliceiri KW. NIH Image to ImageJ: 25 years of image analysis. *Nat Methods* 2012; 9(7): 671–675.
28. Pužar Dominkuš P, Stenovec M, Sitar S, et al. PKH26 labeling of extracellular vesicles: characterization and cellular internalization of contaminating PKH26 nanoparticles. *Biochim Biophys Acta Biomembr* 2018; 1860(6): 1350–1361.
29. Zhao F, Zhou L, Liu J, et al. Construction of a vascularized bladder with autologous adipose-derived stromal vascular fraction cells combined with bladder acellular matrix via tissue engineering. *J Tissue Eng* 2019; 10: 2041731419891256.
30. Gu JW, Young E, Busby B, et al. Oral administration of pyrrolidine dithiocarbamate (PDTC) inhibits VEGF expression, tumor angiogenesis, and growth of breast cancer in female mice. *Cancer Biol Ther* 2009; 8(6): 514–521.
31. Chen Y, Ma D, Wang X, et al. Calnexin impairs the antitumor immunity of $CD4^+$ and $CD8^+$ T cells. *Cancer Immunol Res* 2019; 7(1): 123–135.
32. Hou Y, Li F, Karin M, et al. Analysis of the IKKbeta/NF-kappaB signaling pathway during embryonic angiogenesis. *Dev Dyn* 2008; 237(10): 2926–2935.
33. van Niel G, D'Angelo G and Raposo G. Shedding light on the cell biology of extracellular vesicles. *Nat Rev Mol Cell Biol* 2018; 19(4): 213–228.
34. Shao H, Im H, Castro CM, et al. New technologies for analysis of extracellular vesicles. *Chem Rev* 2018; 118(4): 1917–1950.
35. Phinney DG and Pittenger MF. Concise review: MSC-derived exosomes for cell-free therapy. *Stem Cells* 2017; 35(4): 851–858.
36. Yu X, Huang C, Song B, et al. CD4+CD25+ regulatory T cells-derived exosomes prolonged kidney allograft survival in a rat model. *Cell Immunol* 2013; 285(1–2): 62–68.
37. Wang C, Wang M, Xu T, et al. Engineering bioactive self-healing antibacterial exosomes hydrogel for promoting chronic diabetic wound healing and complete skin regeneration. *Theranostics* 2019; 9(1): 65–76.
38. Li L, Zhang Y, Mu J, et al. Transplantation of human mesenchymal stem-cell-derived exosomes immobilized in an adhesive hydrogel for effective treatment of spinal cord injury. *Nano Lett* 2020; 20(6): 4298–4305.
39. Ju C, Li Y, Shen Y, et al. Transplantation of cardiac mesenchymal stem cell-derived exosomes for angiogenesis. *J Cardiovasc Transl Res* 2018; 11(5): 429–437.
40. Komaki M, Numata Y, Morioka C, et al. Exosomes of human placenta-derived mesenchymal stem cells stimulate angiogenesis. *Stem Cell Res Ther* 2017; 8(1): 219.
41. Harrell CR, Jovicic N, Djonov V, et al. Mesenchymal stem cell-derived exosomes and other extracellular vesicles as new remedies in the therapy of inflammatory diseases. *Cells* 2019; 8(12): 1605.
42. Sharma AK, Bury MI, Marks AJ, et al. A nonhuman primate model for urinary bladder regeneration using autologous sources of bone marrow-derived mesenchymal stem cells. *Stem Cells* 2011; 29(2): 241–250.
43. Nisr RB, Shah DS, Ganley IG, et al. Proinflammatory NFkB signalling promotes mitochondrial dysfunction in skeletal muscle in response to cellular fuel overloading. *Cell Mol Life Sci* 2019; 76(24): 4887–4904.